

# Residual Reinforcement Learning for Robot Teleoperation under Stochastic Delays

Kaize Deng, Zewen Yang<sup>1</sup>

Technical University of Munich, 80333 Munich, Germany  
(e-mail: kaize.deng@tum.de, zewenyang@tum.de).

**Abstract:** Stochastic communication delays in teleoperation introduce signal discontinuities that undermine control stability and degrade control performance. Consequently, the conventional reinforcement learning (RL) methods struggle with the delayed observations due to the delay-induced observations, leading to high-frequency chattering. To address this, we propose a hybrid control framework, delay-resilient RL, integrating a state estimator utilizing Long Short-Term Memory (LSTM) with a residual RL policy, which is resilient to stochastic delays. The LSTM reconstructs smooth, continuous state estimates from delayed observations, enabling the RL agent to learn a residual torque compensation policy that balances tracking accuracy with velocity smoothness. Experimental validation on Franka Panda robots demonstrates that our approach significantly outperforms the state-of-the-art baselines, ensuring robust and stable teleoperation even under high-variance stochastic delays.

*Keywords:* teleoperation system, networked systems, stochastic delay, reinforcement learning

## 1. INTRODUCTION

Teleoperation, a critical technology in modern robotics, enables human operators to control remote manipulators across geographical distances via networked communication. This capability facilitates expert intervention in environments where direct physical presence is impractical or hazardous, spurring transformative applications in domains such as remote surgery (Choi et al., 2018), distributed manufacturing (Manupati et al., 2017), and even space robotic coordination (Ruoff, 1994).

Architecturally, a teleoperation system comprises two primary components: a local leader device, which captures the human operator’s commands, and a remote follower manipulator, which is tasked with executing the corresponding movements in the distant environment (see Fig. 1). First, the networked communication channel between the local and remote sites introduces a stochastic, time-varying state transmission delay. Specifically, the state signal of the leader is sent over the network to the remote reinforcement learning (RL) agent and arrives with a delay  $\omega_s^t \in \mathbb{R}_{\geq 0}$  at time  $t \in \mathbb{R}_{> 0}$ . This information gap fundamentally transforms the problem from a fully observable Markov Decision Process (MDP) into a Partially Observable MDP (POMDP), in which an optimal action cannot be computed directly from the past states. Second, the agent–follower link is subject to inherent bidirectional delays. The observation delay  $\omega_o^t \in \mathbb{R}_{\geq 0}$  affects the sensor feedback from the follower and directly induces delay observability. Therefore, at any time  $t$ , the controller has access only to delayed state information corresponding to  $t - \omega_o^t$ , rather than the true current state of the follower robot. Third, stochastic variability in the action delay  $\omega_a^t \in \mathbb{R}_{\geq 0}$ , commonly referred to as jitter, disrupts

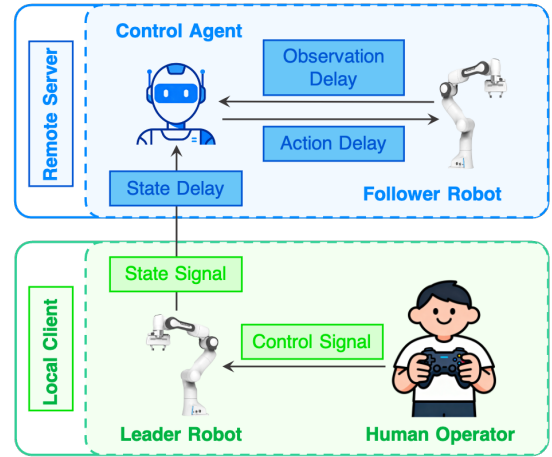


Fig. 1. Teleoperation architecture with stochastic communication delays. The time-varying state delay  $\omega_s^t$  is induced by client-server transmission latency; the action delay  $\omega_a^t$  and observation delay  $\omega_o^t$  arise from the bidirectional delays within the agent–follower control loop.

the command stream along the same agent–follower link. All these factors are particularly detrimental to low-level Proportional–Derivative (PD) control laws, i.e., the asynchronous arrival of commands injects artificial variability into the derivative of the tracking error, thereby inducing high-frequency oscillations, mechanical vibration, and chattering in the closed-loop system.

### 1.1 Related Work

Prior work has addressed the challenges induced by communication delays in teleoperation through several paradigms. Passivity-based control frameworks leverage

<sup>1</sup> Corresponding author (e-mail: zewen.yang@tum.de).

energy conservation principles to establish formal stability guarantees (Niemeyer and Slotine, 1991; Mujčić and Oračević, 2019). By mapping impedance signals into scattering variables, these methods ensure passivity of the communication channel and, by extension, closed-loop stability irrespective of constant delay magnitude. However, the theoretical stability is not guaranteed when delays are stochastic and time-varying rather than constant in real-world networks. Moreover, the requisite signal transformation compromises system transparency, leading to degraded tracking fidelity and attenuated force reflection. Model-based predictive strategies, such as the Smith Predictor (Smith, 1957), attempt to explicitly compensate for latency by simulating the system response forward in time. However, this approach is predicated on accurate a priori knowledge of both plant dynamics and delay characteristics. In scenarios where delays exhibit stochastic variation or significant model–plant mismatch exists, predictive performance deteriorates substantially.

More recent state-of-the-art (SOTA) methods have leveraged RL to tackle these uncertainties. Bypassing the need for such precise, model-based prediction, one category of work uses RL to autonomously tune controller gains (song WANG et al., 2007; Lee et al., 2020; Zhang et al., 2021; Huang et al., 2026). These methods, however, typically model the problem as a MDP, which fundamentally assumes the agent can observe the complete, current state to make an optimal decision. This core assumption is violated by observation delays, where the agent receives only outdated states. Policies trained under this false MDP assumption are thus acting on past information, leading to suboptimal and potentially unstable decisions (Huang et al., 2019; Katsikopoulos and Engelbrecht, 2003).

To address this POMDP, a common strategy is state augmentation (Nath et al., 2021), which stacks past observations and actions into an expanded state representation. However, as delay length grows, the state space expands dramatically, invoking the curse of dimensionality and making learning computationally intractable. Moreover, this fixed-history approach often fails to generalize across variable or highly stochastic delay patterns. Another methodology is model-based Reinforcement Learning (MBRL). The core idea is to learn a predictive model of the environment’s dynamics to compensate for latency (Barde et al., 2020). A naive application, Action-Buffer based State Prediction (ABSP), is computationally prohibitive as it requires re-simulating the entire future trajectory at every time step. To address this inefficiency, the Predictive Model Delay Correction (PMDC) framework (McCutcheon and Fallah, 2023) introduced the more efficient State-Buffer based State Prediction (SBSP). SBSP maintains a buffer of predicted future states and updates it incrementally, making it a computationally viable solution for real-time control. However, despite this computational advance, the SOTA PMDC framework exhibits critical limitations when confronted with high-variance stochastic delays. The framework relies on a single-step state predictor that updates only upon arrival of a new delayed observation; between arrivals, the predictor output is held constant, and at each new arrival, the predicted state jumps discontinuously to incorporate the new measurement. These step-like discontinuities propagate into

the derivative term of the downstream PD law, injecting spurious high-frequency content that destabilizes the control loop regardless of gain adaptation. Furthermore, PMDC’s state prediction lacks explicit velocity learning, resulting in imprecise derivative estimates that compound with delay uncertainty under high-variance conditions. Finally, validation of these advanced predictive methods has been constrained primarily to simulated environments; their robustness and practical applicability on real-world robotic hardware under high-variance network conditions remain largely undemonstrated.

## 1.2 Contributions

To address these persisting research gaps, this paper proposes a hybrid framework that combines a delay-resilient state estimator with a residual reinforcement learning (DR-RL) policy for teleoperation under high-variance stochastic delays. Our primary contributions are:

- **Autoregressive State Estimation for Continuous Predictions:** We develop an LSTM-based state estimator that produces state estimates at a high control rate, decoupling the estimator output frequency from the stochastic and intermittent communication rate. Unlike prior single-step predictors that update only upon packet arrival and produce discontinuous state estimates, our estimator combines a residual update head with an anchored autoregressive rollout, supplying the downstream control loop with kinematically continuous predictions while bounding the accumulated autoregressive drift to the inter-arrival interval of leader observations.
- **Residual Reinforcement Learning for Robust Compensation:** We propose a hybrid control architecture in which a residual RL agent learns corrective torque terms to compensate for model uncertainties and external disturbances. The residual specifically compensates for two sources of controller mismatch observable during simulated training: (1) tracking deviations induced by imperfect predictions from the LSTM estimator under stochastic delay, and (2) residual errors that the underlying PD feedback gains alone are insufficient to suppress.
- **Validation under Diverse Network Conditions:** We validate our framework on a Franka Panda manipulator across three distinct delay scenarios: (1) low delay with low variance, (2) high delay with low variance, and (3) high delay with high variance. This comprehensive evaluation demonstrates practical robustness under varying stochastic communication conditions and addresses a critical gap in the experimental validation of delay-resilient teleoperation methods.

## 2. PRELIMINARY AND PROBLEM SETTING

### 2.1 Teleoperation System

This work considers a homogeneous teleoperation system where the leader ( $l$ ) and follower ( $f$ ) robots share the same embodiment. We model each agent as a rigid-body mechanical system with  $n$  degrees of freedom, whose robot motion equations are described by

$$\mathbf{M}(\mathbf{q})\ddot{\mathbf{q}} + \mathbf{C}(\mathbf{q}, \dot{\mathbf{q}})\dot{\mathbf{q}} + \mathbf{D}\dot{\mathbf{q}} + \mathbf{g}(\mathbf{q}) + \mathbf{d}(\mathbf{q}, \dot{\mathbf{q}}) = \boldsymbol{\tau}, \quad (1)$$

where the  $\mathbf{q} \in \mathbb{R}^n$  is the joint positions, the matrices  $\mathbf{M}(\mathbf{q})$ ,  $\mathbf{C}(\mathbf{q}, \dot{\mathbf{q}})$ , and  $\mathbf{D} \in \mathbb{R}^{n \times n}$  are the inertia, Coriolis/centrifugal, and damping matrices, respectively. The vector function  $\mathbf{g}(\mathbf{q}) \in \mathbb{R}^n$  denotes the gravitational torques, and the control torque vector is  $\boldsymbol{\tau} \in \mathbb{R}^n$ . The external disturbances and model uncertainties are considered in the model as a vector function  $\mathbf{d}(\mathbf{q}, \dot{\mathbf{q}}) \in \mathbb{R}^n$ .

## 2.2 Control Objective

The primary control objective is to achieve high-fidelity motion synchronization between the leader and follower robots. Let  $\mathbf{q}_l(t) \in \mathbb{R}^n$  and  $\mathbf{q}_f(t) \in \mathbb{R}^n$  denote the vector of joint angular positions for the leader robot and the follower robot at time  $t$ , respectively. Since the human operator only controls the end-effector position, the control signal in Fig. 1 is considered as task-space motion. Here, we define the  $\mathbf{x}_l(t) = \mathbf{f}_k(\mathbf{q}_l(t)) \in \mathbb{R}^m$  as the end-effector positions of the local robot, where  $\mathbf{f}_k : \mathbb{R}^n \rightarrow \mathbb{R}^m$  is the forward kinematics mapping.

Therefore, we formally define the joint tracking error  $\mathbf{e}(t)$  as the instantaneous deviation between the leader's and follower's configurations:

$$\mathbf{e}(t) = \mathbf{f}_k^{-1}(\mathbf{x}_l(t)) - \mathbf{q}_f(t). \quad (2)$$

The goal is to design a control policy that minimizes the magnitude of the error  $\mathbf{e}(t)$  under stochastic delays, including state delay  $\omega_s \in \mathbb{R}_{>0}$ , action delay  $\omega_a \in \mathbb{R}_{>0}$ , and observation delay  $\omega_o \in \mathbb{R}_{>0}$ .

## 2.3 State Estimator

Due to the inevitable communication delays between the leader and the follower, obtaining the real-time positions is infeasible. Consequently, the true leader state  $\mathbf{q}_l(t)$ ,  $\dot{\mathbf{q}}_l(t)$  is unobservable at the current time step. The control agent only has access to the delayed states:  $\mathbf{q}_l(t - \omega_s^t)$ ,  $\dot{\mathbf{q}}_l(t - \omega_s^t)$ . However, using this delayed signal in a feedback loop would result in instability. To mitigate this latency and approximate the ground-truth state of the leader robot, we employ a LSTM-based state estimator to reconstruct the real-time leader robot state:  $\hat{\mathbf{q}}_l(t)$  and  $\hat{\dot{\mathbf{q}}}_l(t)$ , which denote the predicted leader states provided by the estimator in Section 3.1.

## 2.4 Controller Design

To track the desired motion of the local leader, a nominal controller based on the computed torque control method is proposed as follows

$$\boldsymbol{\tau}_{\text{nom}} = \mathbf{M}(\mathbf{q}_f)\ddot{\mathbf{q}}_{\text{ref}} + \mathbf{C}(\mathbf{q}_f, \dot{\mathbf{q}}_f)\dot{\mathbf{q}}_f + \mathbf{D}\dot{\mathbf{q}}_f + \mathbf{g}(\mathbf{q}_f), \quad (3a)$$

$$\ddot{\mathbf{q}}_{\text{ref}} = \ddot{\hat{\mathbf{q}}}_l + \mathbf{K}_d(\dot{\hat{\mathbf{q}}}_l - \dot{\mathbf{q}}_f) + \mathbf{K}_p(\hat{\mathbf{q}}_l - \mathbf{q}_f), \quad (3b)$$

where  $\mathbf{K}_p, \mathbf{K}_d \in \mathbb{R}^{n \times n}$  are the positive-definite proportional and derivative gain matrices.

Although the nominal controller provides a robust theoretical basis for trajectory tracking by compensating for known rigid-body dynamics, its efficacy is inherently constrained by unmodeled dynamics and state estimation errors. Inspired by (Johannink et al., 2019), we train a reinforcement learning agent to learn the residual torque compensation term  $\boldsymbol{\tau}_{\text{rl}}$ . Therefore, the final control input

$\boldsymbol{\tau}_{\text{cmd}}$  applied to the follower robot is formulated as the summation of the nominal baseline and the learned residual, i.e.,

$$\boldsymbol{\tau}_{\text{cmd}} = \boldsymbol{\tau}_{\text{nom}} + \boldsymbol{\tau}_{\text{rl}}, \quad (4)$$

where the  $\boldsymbol{\tau}_{\text{rl}}$  is introduced in Section 3.2.

## 3. METHODOLOGY

### 3.1 LSTM-based State Estimator

A critical issue in teleoperation under stochastic delays is the discrete jumps in the feedback signal from the local robot. Such discontinuities result in unbounded derivative estimates in the downstream control loop, regardless of the specific controller used, and induce high-frequency oscillations and chattering. Thus, the estimator must guarantee smooth trajectory reconstruction in addition to minimizing state error, so that the controller can operate on a continuous input signal.

*Residual Update Head* Let the set  $\mathcal{Z}(t)$  denote the sequence of the  $N^t$  most recent delayed states available at time  $t$ :

$$\mathcal{Z}(t) = \{\mathbf{s}_i^t\}_{i=1, \dots, N^t}, \quad (5)$$

where the element  $\mathbf{s}_i^t = [\mathbf{q}_l(t)^\top, \dot{\mathbf{q}}_l(t)^\top, \omega_s^t]^\top$  represents the concatenation of the joint positions  $\mathbf{q}_l(t)$ , velocities  $\dot{\mathbf{q}}_l(t)$ , and the state delay magnitude  $\omega_s^t$ . The LSTM processes this input sequence and maintains an internal recurrent state  $(\mathbf{h}_k, \mathbf{c}_k)$  that summarizes the recent leader motion. The hidden output  $\mathbf{h}_k$  is consumed by the feed-forward head defined below. To design this head, we first observe that the underlying robot dynamics admit an accumulative structure: the transition from state  $\mathbf{s}_{k-1}$  to  $\mathbf{s}_k$  over one integration step is governed by a nonlinear function  $\ell$  representing the rigid-body dynamics and integration scheme,

$$\mathbf{s}_k^t = \mathbf{s}_{k-1}^t + \ell(\mathbf{s}_{k-1}^t) \Delta t \approx \mathbf{s}_{k-1}^t + \Delta \mathbf{s}_{\text{dyn}}, \quad (6)$$

where  $\Delta \mathbf{s}_{\text{dyn}}$  denotes the per-step state change induced by velocity, acceleration, Coriolis forces, and gravity. To mirror this accumulative structure inside the network, we do not let the LSTM regress the next absolute state directly. Instead, a small feed-forward head maps the LSTM hidden representation  $\mathbf{h}_k$  to a learned increment  $\Delta \mathbf{s}_k$ , which is composed with the previous state through an explicit Euler update:

$$\hat{\mathbf{s}}_k = \mathbf{s}_{k-1} + \Delta \mathbf{s}_k, \quad \Delta \mathbf{s}_k = \mathbf{v}_k \cdot \alpha, \quad (7)$$

where  $\mathbf{v}_k$  is the network-predicted velocity correction and  $\alpha \in \mathbb{R}_{>0}$  is a learnable scaling factor. This residual formulation aligns the network output structurally with the rigid-body increment  $\Delta \mathbf{s}_{\text{dyn}}$  in Eq. (6), keeps the regression target well-conditioned over the small per-step magnitude, and guarantees kinematic continuity between consecutive predictions by construction rather than as a soft regularizer in the loss function.

*Autoregressive State Estimation* To generate continuous state estimates at the control rate over extended delay periods, we employ an autoregressive prediction strategy. This mechanism leverages the temporal memory in the LSTM hidden state together with the residual update in Eq. (7) to simulate the robot's forward motion from the most recent anchor observation  $\hat{\mathbf{s}}_k^{(t-\omega_s^t)}$  up to the

current time  $t$ . The prediction horizon is determined by the maximum observed system delay  $\omega_s^{\max}$ . During the delay interval, the estimator performs autoregressive rollouts at the control rate, where the model uses its own previous output as input for the subsequent prediction step:

$$\hat{\mathbf{s}}_k^{(t-\omega_s^t)} = \hat{\mathbf{s}}_{k-1}^{(t-\omega_s^t)} + \Delta \mathbf{s}_k, \quad (8)$$

where  $\Delta \mathbf{s}_k$  is the increment produced by the LSTM head conditioned on the predicted state from the previous iteration and the running hidden state. The autoregressive chain is anchored to the most recent delayed leader observation rather than maintained continuously across the trajectory. Whenever a new delayed observation  $\mathbf{s}^{(t-\omega_s^t)}$  arrives at the agent, the previous autoregressive predictions are discarded and the rollout is re-initialized from this anchor, with the LSTM hidden state correspondingly reset to the value produced by re-encoding the input window terminating at the new anchor.

### 3.2 Residual RL Control

**Observation Space** The presence of stochastic time-varying delay  $\omega_s^t$  inherently renders the environment partially observable, as the agent cannot access the immediate true state of the leader robot. This effectively transforms the standard MDP into a POMDP. A naive approach is State Augmentation (stacking history states into the agent observation space) (Nath et al., 2021), however, this leads to the curse of dimensionality as the required augmentation history length  $N$  grows with delay magnitude. To avoid this computational intractability, we adopt a Model-Based Reinforcement Learning approach. We rely on the LSTM estimator (Section 3.1) to estimate real-time states  $\hat{\mathbf{q}}_l(t)$  and  $\hat{\mathbf{q}}_f(t)$ . This effectively transforms the POMDP into a standard MDP process for the control policy. The RL agent receives an augmented observation vector  $\mathbf{o}_t \in \mathbb{R}^{d_{obs}}$  comprising the follower robot state  $[\mathbf{q}_f, \dot{\mathbf{q}}_f]^T$ , the LSTM-predicted leader state  $[\hat{\mathbf{q}}_l, \dot{\hat{\mathbf{q}}}_l]^T$ , the tracking errors  $[\mathbf{e}_q, \mathbf{e}_{\dot{q}}]^T$ , and the follower state history  $\{\mathbf{q}_f(t-k), \dot{\mathbf{q}}_f(t-k)\}_{k=1}^N$ .

**SAC Algorithm** In this work, we employ Soft Actor-Critic (SAC) for policy optimization due to its sample efficiency and stability in continuous control tasks.

**Objective.** The standard reinforcement learning objective is defined as the expectation of the discounted cumulative reward  $R(\tau) = \sum_{t=0}^T \gamma^t r(\mathbf{s}_t, \mathbf{a}_t)$  over trajectories sampled under the policy  $\pi_\theta$ :

$$J(\theta) = \mathbb{E}_{\tau \sim P_{\pi_\theta}} [R(\tau)]. \quad (9)$$

**Value functions.** To evaluate the policy, SAC relies on the standard state-value and action-value functions:

$$V^\pi(\mathbf{s}) = \mathbb{E}_\pi \left[ \sum_{k=0}^{\infty} \gamma^k r_{t+k} \mid \mathbf{s}_t = \mathbf{s} \right], \quad (10)$$

$$Q^\pi(\mathbf{s}, \mathbf{a}) = \mathbb{E}_\pi \left[ \sum_{k=0}^{\infty} \gamma^k r_{t+k} \mid \mathbf{s}_t = \mathbf{s}, \mathbf{a}_t = \mathbf{a} \right]. \quad (11)$$

The action-value function  $Q^\pi$  serves as the Critic, providing the gradient signal used to improve the actor.

**Entropy-regularized objective.** SAC augments the standard objective with a per-step entropy term  $\mathcal{H}(\pi(\cdot|\mathbf{s}_t))$ :

$$J_{\text{SAC}}(\theta) = \mathbb{E}_{\tau \sim \pi_\theta} \left[ \sum_{t=0}^T \gamma^t (r(\mathbf{s}_t, \mathbf{a}_t) + \alpha \mathcal{H}(\pi(\cdot|\mathbf{s}_t))) \right], \quad (12)$$

where  $\alpha$  is the temperature parameter governing the trade-off between reward maximization and entropy preservation. Maximizing entropy encourages the agent to explore multiple modes of high-reward behavior rather than collapsing into a single deterministic policy, which is particularly important under stochastic delays where the optimal action distribution may be inherently multi-modal.

**Soft Bellman backup.** Under the entropy-regularized objective, the Critic is trained to satisfy the soft Bellman equation, which incorporates the entropy bonus directly into the value backup:

$$Q^\pi(\mathbf{s}, \mathbf{a}) = r + \gamma \mathbb{E}_{\mathbf{s}', \mathbf{a}' \sim \pi} [Q^\pi(\mathbf{s}', \mathbf{a}') - \alpha \log \pi(\mathbf{a}'|\mathbf{s}')], \quad (13)$$

where the prime denotes the next time step. Compared to the standard Bellman backup, the additional term  $-\alpha \log \pi(\mathbf{a}'|\mathbf{s}')$  assigns higher value to states from which the future policy can act with greater entropy.

**Policy improvement.** Given the updated Critic, the actor is improved by projecting the policy onto the distribution induced by the exponentiated soft Q-function:

$$\pi_{\text{new}} = \arg \min_{\pi' \in \Pi} D_{\text{KL}} \left( \pi'(\cdot|\mathbf{s}) \left\| \frac{\exp(Q^\pi(\mathbf{s}, \cdot)/\alpha)}{Z^\pi(\mathbf{s})} \right. \right), \quad (14)$$

where  $Z^\pi(\mathbf{s})$  is the normalization constant. This update preserves entropy in the resulting policy while pulling probability mass towards high-Q actions, yielding the alternating Critic-Actor optimization that defines SAC.

**Multi-Objective Reward Design** The control policy optimization is driven by a composite reward function  $r : \mathcal{S} \times \mathcal{A} \rightarrow \mathbb{R}$ , formulated to balance asymptotic tracking stability with control effort minimization and strict safety constraints. We employ a linear scalarization of these objectives, defined at each time step  $t$  as:

$$r_t(\mathbf{s}_t, \mathbf{a}_t) = r_{\text{track}} + r_{\text{reg}} + r_{\text{safe}}. \quad (15)$$

The tracking fidelity term  $r_{\text{track}}$  penalizes the weighted squared Euclidean distance between the follower joint state and the LSTM-estimated leader joint state:

$$r_{\text{track}} = -\lambda_p \|\hat{\mathbf{q}}_l - \mathbf{q}_f\|_2^2 - \lambda_v \|\hat{\dot{\mathbf{q}}}_l - \dot{\mathbf{q}}_f\|_2^2, \quad (16)$$

where  $\lambda_p, \lambda_v \in \mathbb{R}_{>0}$  are weighting coefficients governing the trade-off between position accuracy and velocity synchronization. The action regularization term  $r_{\text{reg}}$  discourages large residual torques:

$$r_{\text{reg}} = -\lambda_a \frac{1}{n} \sum_{i=1}^n (a_{t,i})^2, \quad (17)$$

where  $a_{t,i}$  is the residual torque applied to joint  $i$ . The safety penalty term  $r_{\text{safe}}$  enforces hard constraints on the agent's behavior as the sum of three per-step penalty terms:

$$r_{\text{safe}} = P_{\text{joint}} + P_{\text{track}} + P_{\text{est}}, \quad (18)$$

where each penalty is independently activated upon violation of its corresponding condition:

$$\begin{cases} P_{\text{joint}} = \rho, & \text{if } \exists i, q_{f,i} \notin [q_{\min}^i, q_{\max}^i], \\ P_{\text{track}} = \rho, & \text{if } \|\mathbf{e}_{\text{track}}\| > \epsilon_{\text{track}}, \\ P_{\text{est}} = \rho, & \text{if } \|\mathbf{e}_{\text{est}}\| > \epsilon_{\text{est}}, \end{cases}, \quad (19)$$

where  $\rho < 0$  is a fixed per-step penalty magnitude, and the three terms accumulate when multiple conditions are

simultaneously violated. The  $[q_{\min}^i, q_{\max}^i]$  denotes the physical limits of the  $i$ -th joint. The tracking error and estimation error, computed during training using the ground-truth leader state available in simulation, are defined as:

$$e_{\text{track}}(k) = \|\mathbf{q}_l(k) - \mathbf{q}_f(k)\|_2, \quad e_{\text{est}}(k) = \|\hat{\mathbf{q}}_l(k) - \mathbf{q}_l(k)\|_2. \quad (20)$$

To stabilize critic learning under the per-step safety penalties, the composite reward  $r_t$  is clipped to a bounded range  $[r_{\min}, r_{\max}]$  during training<sup>2</sup>.

## 4. EXPERIMENTAL RESULTS

### 4.1 Experimental Setup

Our experimental evaluation consists of two parts. First, we conduct a systematic quantitative comparison between DR-RL and two baseline methods in a MuJoCo simulation of the Franka Panda manipulator, evaluated under three stochastic delay configurations (Section 4.2). Second, we deploy the simulator-trained DR-RL policy on the physical Franka Panda manipulator to verify that the framework transfers to real hardware without retraining (Section 4.3).

We systematically compare our method against two baseline approaches:

- **PMDC (SOTA model-based RL method)** (McCutcheon and Fallah, 2023): Utilizes a learned dynamics model and State-Buffer based State Prediction (SBSP) to explicitly estimate the real-time state from delayed observations.
- **Vanilla PD (Baseline method)**: A standard inverse dynamics controller operating directly on delayed observations without prediction or compensation, serving as the performance lower bound.

To quantify the tracking performance, a desired reference trajectory for the end-effector is commanded to the leader robot, which the follower must replicate under delay. The reference trajectory in the task space is defined as

$$\mathbf{x}_l^{\text{ref}}(k) = [0.2 \sin(3k), 0.2 \sin(4k + \frac{\pi}{2}), 0.02 \sin(k)]^\top. \quad (21)$$

The teleoperation system architecture deploys the RL agent co-located with the follower robot, resulting in constant action delay  $\omega_o^t = \omega_a^t = 50$  ms between the agent’s torque commands and the follower robot’s execution for all  $t$ . Stochasticity arises from the network communication between the leader robot and the RL agent, introducing variable observation delay  $\omega_s^t \sim \mathcal{U}(\omega_{\min}, \omega_{\max})$ . The sampling period is set as  $\Delta t = 4$  ms. We evaluate three delay configurations as follows:

- **Low delay with low variance**:  $\omega_s^t \sim \mathcal{U}(120, 160)$  ms, total: 170–210 ms
- **High delay with low variance**:  $\omega_s^t \sim \mathcal{U}(200, 240)$  ms, total: 250–290 ms
- **High delay with high variance**:  $\omega_s^t \sim \mathcal{U}(40, 240)$  ms, total: 90–290 ms

These three delay configurations are used both in the simulation comparison and in the physical-robot deployment of DR-RL, allowing a consistent evaluation of the framework across the operating envelope of stochastic delays considered in this work.

<sup>2</sup> The detailed training hyperparameters are listed in Appendix A

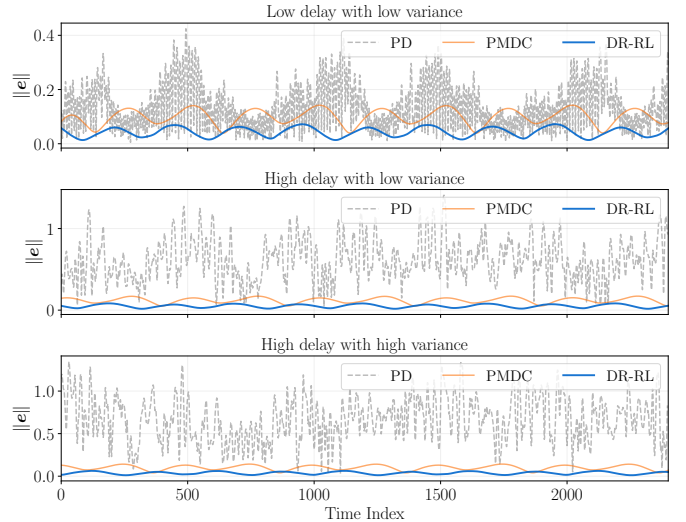


Fig. 2. Tracking error  $\|\mathbf{e}\|$  comparison against other methods under different network delay conditions.

### 4.2 Quantitative Comparison in Simulation

We evaluate the tracking performance by the norm of the Cartesian tracking error  $\|\mathbf{e}(t)\|$  between the leader and follower end-effectors, computed over the first 50 s of each trial<sup>3</sup>. In Fig. 2, it is shown that in all three scenarios, DR-RL is superior to PD and PMDC methods. Under low-delay, low-variance conditions (170–210 ms), DR-RL achieves the lowest tracking error, outperforming both PMDC and the Vanilla PD controller, which exhibits substantial oscillations (peaks  $\approx 0.4$  m); this demonstrates the superiority of LSTM-based autoregressive estimation over feedforward networks used in PMDC. As delay magnitude increases to 250–290 ms, DR-RL maintains stable, low-error performance, whereas PMDC deteriorates and the PD controller fails completely with error peaks exceeding 1 m. The most pronounced differentiation emerges under the challenging high-delay, high-variance scenario (90–290 ms): the PD controller exhibits severe instability with consistent oscillation, and PMDC degrades significantly due to the inability of its memoryless feedforward network to adapt to variable delays from fixed-length inputs.

### 4.3 Real-Robot Deployment

To verify that the simulator-trained DR-RL policy transfers to physical hardware, we deploy the same policy and estimator weights used in the simulation study on a physical Franka Panda manipulator, with no additional fine-tuning or calibration on real-robot data. Table 1 reports the resulting sim-to-real tracking error under the high-delay, high-variance configuration (90–290 ms), which corresponds to the hardest of the three settings evaluated in the simulation.

The mean Cartesian tracking error increases from 0.037 m in simulation to 0.045 m on hardware, a relative degradation of approximately 22%. The maximum error rises by a similar factor. This bounded sim-to-real gap reflects three properties of the proposed framework. First, the LSTM

<sup>3</sup> The additional results are available in Appendix B.

Table 1. Sim-to-real tracking error comparison of DR-RL under the high-delay, high-variance delays.

	Sim	Real	Ratio
Mean (m)	0.037	0.045	1.22×
Max (m)	0.063	0.078	1.24×

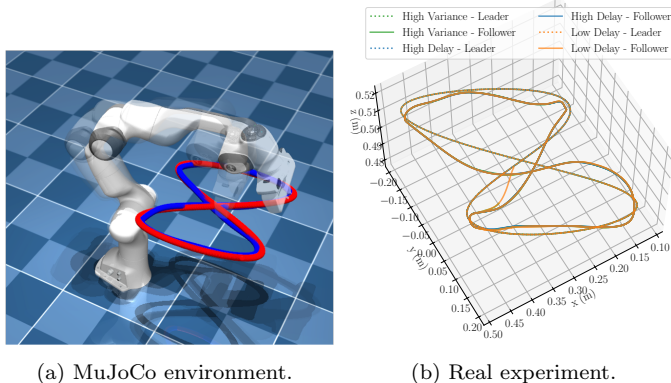


Fig. 3. Visualization of spatial trajectories using DR-RL in a high-delay, high-variance scenario. (a) The red line is the local leader, the blue line denotes the remote follower. (b) The dashed line is the leader, while the solid line is the follower.

estimator operates only on leader-side kinematic trajectories, which are independent of follower-robot dynamics and therefore consistent between simulation and physical deployment. Second, the nominal computed-torque controller in Eq. (3a) is parameterized with manufacturer-calibrated dynamics that are also used directly in the MuJoCo simulator, eliminating the inertial mismatch that typically dominates sim-to-real degradation in residual learning frameworks. Third, the residual RL policy learns only a small torque correction on top of the nominal controller, bounding the magnitude by which sim-trained behavior can degrade under unmodeled real-world dynamics. The corresponding spatial trajectory on the physical manipulator is shown in Fig. 3b.

## 5. CONCLUSION

This paper introduces DR-RL, a hybrid learning-based control framework for robust teleoperation under high-variance stochastic delays. At its core is an autoregressive state estimator that leverages LSTM-based temporal memory to resolve delay-induced partial observability, while a coupled residual reinforcement learning policy compensates for unmodeled dynamics to ensure stable and precise operation. Experimental validation on a physical Franka Panda demonstrates that our framework significantly outperforms SOTA baselines, achieving superior tracking performance and stability.

## REFERENCES

Barde, P., Roy, J., de La Saulece, É., Calauzènes, C., and Moinard, V. (2020). At human speed: Deep reinforcement learning with action delay. In *International Conference on Learning Representations*.  
 Choi, P.J., Oskouian, R.J., and Tubbs, R.S. (2018). Telesurgery: Past, Present, and Future. *Cureus*, 10(5).

Huang, B., Gong, Y., Yang, Z., Ren, T., and Figueredo, L. (2026). Contact-Safe Reinforcement Learning with ProMP Reparameterization and Energy Awareness.  
 Huang, J., Chen, J., and Sun, C. (2019). Reinforcement learning in robotic teleoperation with time delay: A survey. *Annual Reviews in Control*, 48, 189–203. doi: 10.1016/j.arcontrol.2019.06.005.  
 Johannink, T., Bahl, S., Nair, A., Luo, J., Kumar, A., Loskyll, M., Ojea, J.A., Solowjow, E., and Levine, S. (2019). Residual Reinforcement Learning for Robot Control. In *2019 International Conference on Robotics and Automation (ICRA)*, 6023–6029. doi: 10.1109/ICRA.2019.8794127.  
 Katsikopoulos, K.V. and Engelbrecht, S.E. (2003). Markov decision processes with delays and asynchronous cost collection. *IEEE Transactions on Automatic Control*, 48(4), 568–574. doi:10.1109/TAC.2003.809800.  
 Lee, D., Lee, S.J., and Yim, S.C. (2020). Reinforcement Learning-Based Adaptive PID Controller for DPS. *Ocean Engineering*, 216, 108053.  
 Manupati, V.K., Krishnan, M.G., Varela, M.L.R., and Machado, J. (2017). Telefacturing based distributed manufacturing environment for optimal manufacturing service by enhancing the interoperability in the hubs. *Journal of Engineering*, 2017, 1–14. doi: 10.1155/2017/9305989.  
 McCutcheon, L. and Fallah, S. (2023). Adaptive PD Control Using Deep Reinforcement Learning for Local-Remote Teleoperation with Stochastic Time Delays. In *2023 IEEE/RSJ International Conference on Intelligent Robots and Systems (IROS)*, 7046–7053. doi: 10.1109/IROS55552.2023.10341953.  
 Mujčić, E. and Oračević, A. (2019). Internet Based Teleoperations With Using Wave Variables. *Not specified in paper*. Appears to be a conference or journal publication.  
 Nath, S., Baranwal, M., and Khadilkar, H. (2021). Revisiting State Augmentation Methods for Reinforcement Learning with Stochastic Delays. In *Proceedings of the Association for Computing Machinery*, 1346–1355. doi: 10.1145/3459637.3482386.  
 Niemeyer, G. and Slotine, J.J. (1991). Stable Adaptive Teleoperation. *IEEE Journal of Oceanic Engineering*, 16(1), 1619–1625.  
 Ruoff, C. (1994). *Teleoperation and Robotics in Space (Ingeniería Mecánica y Maquinaria)*. American Institute of Aeronautics & Astronautics.  
 Smith, O.J.M. (1957). Closed Control of Loops with Dead Time. *Chemical Engineering Progress*, 53(5), 217–219.  
 WANG, X., hu CHENG, Y., and SUN, W. (2007). A proposal of adaptive pid controller based on reinforcement learning. volume 17, 40–44. Elsevier. doi: 10.1016/S1006-1266(07)60009-1.  
 Zhang, H., Yang, Y., and Jiang, Y. (2021). Reinforcement learning-based control with communication delays: Theory and applications. *IEEE Transactions on Cybernetics*, 51(9), 4368–4381. doi:10.1109/TCYB.2020.2988820.

## Appendix A. TRAINING PROCEDURE

The proposed framework is trained in two stages, both conducted entirely within a MuJoCo simulation of the Franka Panda manipulator. No real-robot data is used during training; the physical experiments described in Section 4.2 therefore also serve as a sim-to-real evaluation. Training and validation environments are instantiated from distinct random seeds to prevent data leakage.

**Training data and collection.** The training data consists of figure-8 reference trajectories generated on-the-fly by the leader simulator, with their geometric and temporal parameters randomized at each episode reset (center  $c_x \in [0.3, 0.4]$  m,  $c_y \in [-0.1, 0.1]$  m, scale  $s_{x,y} \in [0.1, 0.3]$  m,  $s_z \in [0.01, 0.03]$  m, frequency  $f \in [0.05, 0.15]$  Hz). At every control step, the leader joint state, the corresponding stochastic delay  $\omega_s^t$ , and the future ground-truth trajectory used as the autoregressive target are written into a circular replay buffer. This online collection scheme is chosen over a pre-collected fixed dataset for two reasons. First, the joint distribution of trajectory shape and delay realization is too high-dimensional to enumerate offline; sampling on-the-fly ensures uniform coverage of the operating envelope used at deployment. Second, the autoregressive target tensor (245 future steps per sample) makes a fully materialized dataset prohibitively large; the buffer keeps only the most recent samples and overwrites older ones, providing a near-uniform on-policy distribution at constant memory cost.

**Estimator training.** In the first stage, the LSTM estimator is trained to minimize the mean squared error between its autoregressive rollout and the ground-truth trajectory over the AR horizon. A naive autoregressive loss diverges in practice because the network never receives its own (initially poor) predictions during training; we therefore employ scheduled sampling, starting from full teacher forcing and decaying the ground-truth probability geometrically per update. This gradually exposes the network to its own error distribution and stabilizes long-horizon rollouts. Early stopping is governed by a closed-loop validation rollout in which the estimator is plugged into the simulation and the resulting prediction error is monitored, so that the validation metric reflects deployment-time performance rather than open-loop one-step accuracy.

**Policy training.** In the second stage, the residual SAC policy is trained with the LSTM estimator weights frozen, so that the policy treats the estimator as a fixed component of the environment. Predicted leader states are supplied as part of the observation vector defined in Section 3.2. Transitions collected during the warm-up phase are excluded from the replay buffer because the leader state history during this period is incomplete and would bias the value estimates. The best-performing checkpoint is retained based on the mean return of deterministic validation rollouts. Key hyperparameters of both stages are summarized in Table A.1.

## Appendix B. ADDITIONAL RESULTS

To visualize the three delay configurations in Fig. B.1.

Table B.1 summarizes the mean, 95th percentile (P95), maximum, and standard deviation of  $\|e(t)\|$  for DR-RL,

Table A.1. Key training hyperparameters of the LSTM estimator and the residual SAC policy.

Parameter	Value
<i>LSTM estimator</i>	
Hidden dim. / layers	256 / 3
Output head activation	Mish
Input seq. length	150 steps (600 ms)
AR rollout horizon	245 steps ( $\approx 980$ ms)
Learning rate / batch size	$5 \times 10^{-4}$ / 256
Total updates	500,000
Scheduled sampling decay	0.99995 per update
<i>Residual SAC policy</i>	
Hidden dims (actor / critic)	[512, 256]
LR (actor / critic / $\alpha$ )	$3 \times 10^{-5}$ / $3 \times 10^{-5}$ / $3 \times 10^{-4}$
Discount $\gamma$ / soft update $\tau$	0.99 / 0.005
Batch size / buffer size	128 / $1 \times 10^6$
Total environment steps	$3 \times 10^6$
Reward weights ( $\lambda_p, \lambda_v, \lambda_a$ )	10, 5, 0.01
Safety thresholds ( $\epsilon_{\text{track}}, \epsilon_{\text{est}}$ )	0.5, 0.3 rad
Safety penalty $\rho$	-5
Reward clip range ( $r_{\min}, r_{\max}$ )	[-20, 5]
<i>Common</i>	
Optimizer	Adam
Control frequency	250 Hz ( $\Delta t = 4$ ms)

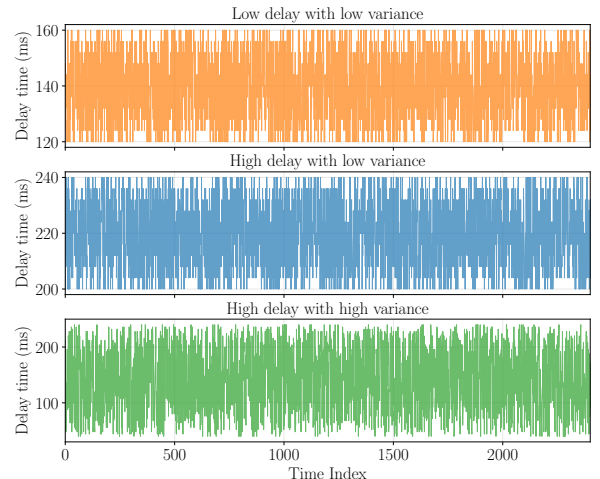


Fig. B.1. State delay patterns in teleoperation tasks. Low delay with low variance (top), high delay with low variance (middle), high delay with high variance (bottom).

PMDC, and the Vanilla PD baseline across all three delay configurations.

Across all three configurations, DR-RL achieves the lowest mean tracking error, reducing the mean by approximately 58–64% relative to the SOTA model-based RL baseline (PMDC). The improvement is consistent across percentiles: the 95th-percentile error of DR-RL is below the mean error of PMDC in every configuration, indicating that DR-RL’s worst-case behavior out-performs PMDC’s average-case behavior under the same delay conditions. Under low delay with low variance (170–210 ms), DR-RL attains a mean error of 0.036 m versus 0.099 m for PMDC in . As the delay magnitude increases to 250–290 ms (high / low variance), the Vanilla PD baseline fails completely

Table B.1. Tracking error metrics in simulation.

Condition / Method	Mean (m)	P95 (m)	Max (m)
<i>Low / low var.</i>			
DR-RL	<b>0.036</b>	<b>0.059</b>	<b>0.062</b>
PMDC	0.099	0.139	0.142
PD	0.24	0.371	0.509
<i>High / low var.</i>			
DR-RL	<b>0.050</b>	<b>0.079</b>	<b>0.083</b>
PMDC	0.119	0.168	0.172
PD	0.618	1.091	1.409
<i>High / high var.</i>			
DR-RL	<b>0.037</b>	<b>0.060</b>	<b>0.063</b>
PMDC	0.100	0.140	0.142
PD	0.671	1.098	1.346

with maximum errors exceeding 1.4 m, while DR-RL remains stable at 0.050 m mean error. Under the most challenging configuration of 90–290 ms (high / high variance), PD continues to exhibit severe oscillations and PMDC degrades to 0.100 m mean error, whereas DR-RL maintains 0.037 m. This robustness under high-variance delay reflects the combined effect of the autoregressive LSTM estimator, which supplies continuous predictions at the control rate, and the torque-level residual policy, which compensates for the residual model uncertainty rather than relying on gain adaptation.